ELSEVIER

Agricultural and Forest Meteorology 102 (2000) 187–206

AGRICULTURAL AND FOREST METEOROLOGY

www.elsevier.com/locate/agrformet

On measuring and modeling energy fluxes above the floor of a homogeneous and heterogeneous conifer forest

Dennis D. Baldocchi [a,*], Beverly E. Law [b], Peter M. Anthoni [b]

[a] *Department of Environmental Science, Ecosystem Science Division, Policy and Management, 151 Hilgard Hall, University of California, Berkeley, CA 94720, USA*

[b] *Department of Forest Science, 154 Peavy Hall, Oregon State University, Corvallis, OR 97331, USA*

Received 14 May 1999; received in revised form 10 December 1999; accepted 17 December 1999

Abstract

Information on mass and energy exchange at the soil surface under vegetation is a critical component of micrometeorological, climate, biogeochemical and hydrological models. Under sparse boreal and western conifer forests as much as 50% of incident solar energy reaches the soil surface. How this energy is partitioned into evaporating soil moisture, heating the air and soil remains a topic of scientific inquiry, as it is complicated by such factors as soil texture, litter, soil moisture, available energy, humidity deficits and turbulent mixing.

Fluxes of mass and energy near the forest floor of a temperate ponderosa pine and a boreal jack pine stand were evaluated with eddy covariance measurements and a micrometeorological soil/plant/atmosphere exchange model. Field tests showed that the eddy covariance method is valid for studying the mean behavior of mass and energy exchange below forest canopies. On the other hand, large shade patches and sunflecks, along with the intermittent nature of atmospheric turbulence, cause run-to-run variability of mass and energy exchange measurements to be large.

In general, latent heat flux densities are a non-linear function of available energy when the forest floor is dry. Latent heat flux densities (λE) are about one-quarter of available energy, when this energy is below $100\,W\,m^{-2}$. Latent heat flux density (λE) peaks at about $35\,W\,m^{-2}$ when available energy exceeds this threshold. A diagnosis of measurements with a canopy micrometeorological model indicates that the partitioning of solar energy into sensible, latent and soil heat flux is affected by atmospheric thermal stratification, surface wetness and the thickness of the litter layer.

Keywords: Soil evaporation; Ponderosa pine; Jack pine; Micrometeorology; Biosphere–atmosphere interactions; BOREAS

1. Introduction

A forest canopy is a dual source system, as its vegetation and underlying soil surface contribute, in differing but significant amounts, to mass and energy exchange between the biosphere and atmosphere. As a first approximation, the rates of latent and sensible heat exchange, occurring at the soil surface, are proportional to that amount of solar energy intercepted by the soil (Ritchie, 1972; Shuttleworth and Wallace, 1985; Villalobos and Fereres, 1990; Brenner and Incoll, 1997). Consequently, the energy fluxes at the soil surface will scale inversely with leaf area index. This is because the relative fraction of light interception by

* Corresponding author.
E-mail addresses: baldocchi@nature.berkeley.edu (D.D. Baldocchi), lawb@ccmail.orst.edu (B.E. Law)

0168-1923/00/$ – see front matter
PII: S0168-1923(00)00098-8

the soil decreases exponentially as the leaf area (L) of the canopy increases:

$$\frac{I(L)}{I(0)} = \exp(-kL) \quad (1)$$

where k is the light extinction coefficient (Ross, 1976). Additional factors affecting rates of mass and energy exchange at the soil–atmosphere interface include soil organic matter content, texture, bulk density and water content, the presence or absence of litter, albedo, wind speed, air temperature and humidity (Villalobos and Fereres, 1990; Wallace et al., 1993; Milhailovic et al., 1995; Cellier et al., 1996; Daamen and Simmonds, 1996).

Scientific studies on mass and energy exchange over bare soil have been conducted since the first half of this century (e.g. Penman, 1948; Philip, 1957). And today, studies on this topic remain an area of active research (e.g. Milhailovic et al., 1995; Cellier et al., 1996; Daamen and Simmonds, 1996; Boulet et al., 1997). One objective of contemporary studies on soil mass and energy exchange involves parameterizing soil–vegetation–atmosphere-transfer (SVAT) algorithms that are incorporated into climate, meteorology and hydrology models (Shuttleworth, 1991; Sellers et al., 1997). Information on CO_2, water vapor and sensible heat exchange from the soil under forests and crops is also needed to evaluate canopy transpiration and net primary productivity (e.g. Wallace et al., 1993; Baldocchi and Vogel, 1996; Baldocchi et al., 1997; Saugier et al., 1997).

One should not expect mass and energy exchange over soil below vegetation to proceed at the same rates as over bare agricultural fields. First, litter covers forest soils and its presence insulates the soil, alters its albedo and affects the diffusion of heat and moisture. For example, litter has a higher albedo, a lower thermal conductivity and a greater amount of pore space than soil. The presence of an overlying vegetation canopy also affects how the soil surface is ventilated, how much solar energy is received at the atmosphere–soil interface and the temperature and atmospheric humidity deficit that is in contact with the soil surface. Compared with literature on mass and energy exchange over bare soil, relatively few studies report direct measurements of the rates and the controlling processes over the soil system under vegetated canopies (e.g. Walker, 1983; Denmead, 1984; Black and Kelliher, 1989; Villalobos and Fereres, 1990; Kelliher et al., 1990, 1997, 1998; Baldocchi and Meyers, 1991; Wallace et al., 1993; Sauer et al., 1995; Baldocchi and Vogel, 1996). Consequently, there is wide conjecture about how different environmental variables contribute to evaporation, sensible heat convection and soil heat conduction at the soil-air interface. The simplest algorithms assume evaporation is a function of net radiation and the number of days since it rained (Ritchie, 1972; Denmead, 1984; Kelliher et al., 1998). Yet, micro-lysimeter (Black and Kelliher, 1989; Kelliher et al., 1990, 1997; Villalobos and Fereres, 1990; Wallace et al., 1993) and eddy covariance (Baldocchi and Meyers, 1991) studies show that the coupling between evaporation and available energy depends upon whether the soil surface is wet and on the amount of turbulent mixing. Over dry soil surfaces, the proportionality between evaporation and available energy is small, though the correlation between these dependent and independent variables is strong (Black and Kelliher, 1989; Baldocchi and Meyers, 1991; Kelliher et al., 1997). Large scale eddies occur with enough frequency to sweep out the moisture in the canopy air space before evaporation rates can come into equilibrium with the demand set by available energy (Baldocchi and Meyers, 1991).

Physically based soil evaporation models originate from theories first proposed by Philip (1957). These models evaluate soil evaporation as a function of the product between the surface conductance and the humidity gradient (e.g. Choudhury and Monteith, 1988; Kondo et al., 1990; Mahfouf and Noilhan, 1991; Milhailovic et al., 1995; Daamen and Simmonds, 1996; Milhailovic and Kallos, 1997). This approach, however, needs an independent means for estimating the surface resistance (R_{soil}) and the vapor pressure in the soil matrix ($e(T_s)$). In the past decade, several groups have developed theoretical algorithms that define R_{soil} and $e(T_s)$ as a function of soil moisture content (Kondo et al., 1990; Mahfouf and Noilhan, 1991). Yet, these schemes have not been widely tested under vegetated canopies. Most field tests of these algorithms pertain to studies over bare soil (Braud et al., 1993; Milhailovic et al., 1995; Daamen and Simmonds, 1996; Boulet et al., 1997).

Western temperate and boreal conifer forests possess relatively low leaf area indices (Runyon et al., 1994; Chen, 1996). Therefore, one should expect, a

priori, that significant amounts of mass and energy exchange occur at the soil surface. The presence of lichen, dead needles, and mosses and the mosaic of sun and shade patches further complicate mass and energy exchange over the soil surface of western and boreal conifer forests.

During the summer of 1994, we measured mass and energy exchange under a boreal jack pine stand (*Pinus banksiana*) using the eddy covariance method, as part of the BOREAS project. In 1996 and 1997, we repeated the experiment in an old growth ponderosa pine (*P. ponderosa*) forest, in Central Oregon. While the leaf area index of both study sites was relatively low, the spatial distribution of stems differed greatly (Table 1). The boreal forest stand was relatively homogeneous and dense (>1800 stems per ha). In contrast, the ponderosa pine stand was extremely open and heterogeneous, as it contained a mix of young and old growth trees (555 young and 72 old-growth trees per ha).

The goals of this paper are threefold. First, we examine the application of the eddy covariance method to measure and interpret mass and energy fluxes under conifer forests. Next, we examine how environmental variables control mass and energy exchange at the floor of these two forest stands. Finally, we use the field measurement data to test the ability of the CANVEG model (Baldocchi and Meyers, 1998) to compute mass and energy fluxes at the soil surface under a conifer forest stand. We then use model computations to help us interpret our field measurements.

Information on CO_2 exchange under these forests is reported elsewhere (Law et al., 1999a).

2. Materials and methods

2.1. Site characteristics

2.1.1. Boreal jack pine

The first study was conducted under a stand of jack pine (*P. banksiana*). The forest study site was near Nipawin, Sask., Canada (53°54′58.82″N, 104°41′31.29″W; elevation 579.3 m). This site is located in the southern portion of the boreal forest. In this region, the vegetation consists of pure and mixed stands of black and white spruce, aspen, jack pine and fen. Jack pine stands tend to be found on well-drained and nutrient-poor sites that burn occasionally.

Field measurements commenced in the spring (23 May 1994) and continued past the first frost and well into the autumnal period, when leaves on local deciduous trees and shrubs and annual herbs were senescing and abscising (16 September 1994). Climate records from nearby, Prince Albert National Park (53°13′N, 105°41′W) show that 259 mm of precipitation fall, on average, during the growing season (May–September). Daily minimum temperature, dur-

Table 1
Site information for the two conifer field studies

Site	Nipawin, Saskatchewan	Metolius Natural Research Area, OR	
Species	*Pinus banksiana*	*Pinus ponderosa*	
Latitude	53°54′58.82″N	44.489°N	
Longitude	104°41′31.29″W	121.65°W	
Leaf area	1.89–2.22	1.53	
Annual precipitation (mm)	398	570 (Sisters, OR)	
Mean temperature (°C)	0.1	8.66 (Metolius, OR)	
Bulk density ($g\,cm^{-3}$)	1.36–1.51	1.05	
		Young Stand (40%)	Old Stand (60%)
Tree height (m)	13.5	9	33
Diameter breast height (m)	0.117	0.12	0.63
Basal area ($m^3\,ha^{-1}$)	21.9	7.1	25.3
Stems per hectare	1875	550	70
Soil Nitrogen ($\mu g\,g^{-1}$)	109–308	149	980
Humus Nitrogen ($\mu g\,g^{-1}$)		974	592
Annual litterfall biomass ($g\,m^{-2}$)		500	310

ing this period, ranged between 2.6 and 10.6°C and daily maximum air temperatures ranged between 16.4 and 24.2°C. The mean annual precipitation of the region is 398 mm and the mean annual temperature is 0.1°C. The region receives about 2570 MJ m^{-2} per year of photosynthetically active radiation.

The terrain and the field site were ideal for applying the micrometeorological eddy covariance method. The terrain was relatively flat (its mean slope in the vicinity of the site ranged between 2 and 5%) and the jack pine forest extended for over a kilometer in all directions.

The stand was mono-specific. Its age ranged between 75 and 90 years old. The stand density was 1875 stems ha^{-1}, its mean diameter at breast height was 0.117 m, and its basal area was 21.9 m^2 ha^{-1}. The height of the canopy ranged between 12 and 15 m and its mean height was 13.5 m (Chen, 1996). The leaf area index (one-half of total surface area of needles per unit ground area) ranged between 1.89 and 2.27 (Chen, 1996). The needle to shoot area ratio ranged between 1.28 and 1.51 and the element-clumping index was 0.71.

The understory vegetation was sparse. However, there were isolated groups of alder (*Alnus crispa*). The ground cover was extensive (nearly 100%) and consisted of bearberry (*Arctostaphylos uva-ursi*), bog cranberry (*Vaccinium vitisideae*), and lichens (*Cladina* spp.). During the middle of the growing season, an herb, *Apocynum*, was present near the ground.

The soil was a course textured sand and was classified as a degraded Eutric Brunisol/Orthic Eutric Brunisol. In summary, the soil was well drained and contained relatively little carbon and nitrogen. During the intensive field campaigns, volumetric soil moisture was measured every other day. Over the course of the experiment, volumetric soil moisture, ranged between 4 and 16% in the layer between 0 and 0.15 m (Cuenca et al., 1997). Soil moisture at a depth of 1.25 m varied less and ranged between 8 and 16%.

2.1.2. Western ponderosa pine forest

The second study was performed under a ponderosa pine forest (*P. ponderosa*) in the Metolius Research Nature Area of Deschutes National Forest near Camp Sherman, OR (latitude 44.489°N; longtitude 121.65°W, elevation 941 m). Ponderosa pine is a wide ranging species in western North America (Elias, 1980; Smith, 1985). These forests exist in continental montane habitats, which are subject to considerable seasonal variation in climate. They are typically exposed to freezing winter temperatures, low annual precipitation (<600 mm per year) and large soil water deficits and vapor pressure deficits during the growing season (Franklin and Dyrness, 1973). These forest stands are typically open, and include varying amounts of understory shrubs (*Purshia tridentata*, *Arctosaphyollos patula*), herbs (*Frageria vesca*), and forbs (*Festuca idahoensis*). With the exclusion of fire, the forests have more shrub cover and include Douglas fir (*Pseudotsuga menziesii*) and grand fir (*Abies grandis*).

The forest stand under investigation contained widely-spaced, old-growth pine (250 years old and 27% of the land area), denser patches of younger trees (45 years old and 25% of the land area) and old/young mixed stands (48% of the land area). The mean canopy height of the young trees was 10 m, and the old growth trees averaged 34 m in height. The mean leaf area index of the stand was estimated to be 1.53, using a remotely sensed optical method (LAI-2000; LICOR, Lincoln, NE). This value represents one-half total surface area of needles per ground area and is uncorrected for clumping. The needle to shoot area ratio was 1.29 and the element-clumping index was 0.86, as determined from tree dimension measurements and a three-dimensional radiative transfer model (Law et al., in preparation). Because of the reintroduction of fire, the understory was relatively sparse, with areas of bracken ferns (*Pteridium aquilinum*), bitterbrush (*Pu. tridentata*) or strawberry (*F. vesca*). The fractional coverage of the soil by the herbs was between 20 and 30%.

The soil is sandy loam and is classified as light-colored, andic inceptisol. It is high in ash, low in nutrients. The soil contained 73% sand, 21% silt, 6% clay (Law et al., 1999b). Organic matter content, to 30 cm depth, is 2.9%, bulk density is 1.05 and soil water holding capacity to 1 m depth is 163 mm (S. Remillard, personal communication). Surface litter was scant in the old-age stands (194 g m^{-2}), and averaged 38% lower than in the young stands (315 g m^{-2}). Soil water content over the year ranged between 0.07 and 0.14 m^3 m^{-3} in the layer between the surface and 0.3 m depth from June to September (Table 2).

The region experiences ~2300 MJ m^{-2} of photosynthetically active radiation over a year (Runyon

Table 2
Soil water content ($m^3\,m^{-3}$) and standard deviation at ponderosa pine field site[a]

Day	SWC (30 cm)	SWC (30 cm S.D.)	SWC (100 cm)	SWC (100 cm S.D.)
181	0.132	0.016	0.153	0.025
193	0.112	0.016	0.147	0.021
194	0.121	0.024	0.148	0.019
198	0.109	0.016	0.137	0.018
210	0.087	0.007	0.127	0.016
232	0.078	0.014	0.112	0.016

[a] Measurements were made with a time domain reflectometer.

et al., 1994; Law et al., 2000). Thirty-year climatic measurements from the Sisters, OR weather station, 13 km southeast of the field site, records a mean annual temperature of 8.66°C and a mean annual precipitation of 360 mm. July and August are typically warm (mean temperature, 18°C) and dry (<15 mm of rainfall per month). In 1996, total precipitation was 595 mm, with no precipitation in July and August.

The terrain and fetch within the study area were satisfactory for conducting micrometeorological experiments. The terrain was relatively flat (2–6% slopes) and the overstory ponderosa pine forest extended more than 10 km in all directions. The only terrain complexity was an abrupt, north–south, running ridge that was about 1 km east of the field site.

Table 1 summarizes the climate and structural characteristics of each field site. The marked differences in canopy structure and climate had a significant impact on wind speed sensed near the floor of the two forests (Fig. 1). The probability distribution of wind speed under the jack pine stand was positively skewed and had a mode near 0.20 m s^{-1}. In contrast, the distribution of wind speed under the ponderosa pine stand was more symmetric and had a mode near 0.50 m s^{-1}.

2.2. Instrumentation

Carbon dioxide, water vapor and sensible heat fluxes were measured using an eddy covariance flux system. The eddy flux systems were positioned near the floor of the canopy and in the stem space of the canopy, where virtually no foliage was present between the canopy floor and the measurement height. The instruments were placed 1.8 m above the ground during the boreal forest study and were 2.52 m above ground during the ponderosa pine experiment.

Wind velocity and virtual temperature fluctuations were measured with a three-dimensional sonic anemometer (an Applied Technology Inc, model SWS-211/3K anemometer was used for the boreal forest study and a Gill Instruments Ltd, Solent anemometer UK was employed during for the ponderosa pine study). CO_2 and water vapor fluctuations were measured with an open-path, infrared absorption gas analyzer (Auble and Meyers, 1992). The water vapor and CO_2 sensor responds to frequencies up to 15 Hz, has a low noise to signal ratio and is rugged and water proof. Standard mixtures of carbon dioxide were used for calibration. These gases were traceable to standards maintained by the World Meteorological Organization (WMO) (Zhao et al., 1997).

The flux measurement system, consisting of a lap top computer, a sonic anemometer and the CO_2/water vapor sensor, drew about 3.8 A of 12 V DC current.

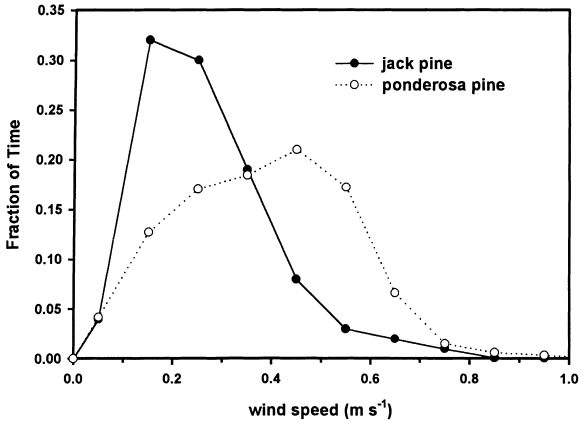

Fig. 1. The probability distribution of wind speed measured at 2 m above the ground in the understory of a boreal jack pine and a temperate ponderosa pine forest.

Analog sensor signals were digitized at 10 Hz with hardware on the sonic anemometer. Micrometeorological flux data were processed and stored on the computer using in-house software. The eddy covariance flux system was powered with AC electricity during the BOREAS study and with solar panels during the Oregon study. The solar-powered electrical generation system consisted of seven Seimens solar panels (Model M75, rated for 48 W and 3.02 A), a photovoltaic controller (Morningstar, Prostar 30) and four deep cycle, 12 V marine batteries, which were connected in parallel. The solar panels were placed in a clearing at the forest floor, 20 m south of the flux system. With this configuration, the electrical energy power system could generate up to about 17 A in full sun and was able to store and re-charge the batteries over the course of 24 h.

Soil heat flux density was measured by averaging the output of three soil heat flux plates (model HFT-3, REBS, Seattle, WA). They were buried 0.01 m below the surface and were randomly placed within a few meters of the flux system. Soil temperature was measured with two, home-made, multi-level thermocouple probes. Sensors were spaced logarithmically at 0.02, 0.04, 0.08, 0.16 and 0.32 m below the surface.

Photosynthetically active photon flux density (Q_p) and the net radiation balance were measured above the soil and forest with a quantum sensor (model LI-190S, LICOR, Lincoln, NE) and a net radiometer (Model 6, REBS, Seattle, WA), respectively. To account for sampling errors due to the high spatial variability of the forest radiation climate, the solar radiation instruments were mounted on a tram that traversed across the forest understory. In the case of the jack pine stand, a 14.5 m path length was used. A longer traversing path (36 m) was employed to measure the solar radiation field under the ponderosa pine. The length of the horizontal transect was chosen to minimize the coefficient of variation of the spatial sample to within 20%. The translation velocity and sampling rates were designed so a sample was taken every millimeter (0.1 s sample frequency, 1 cm s^{-1} travel velocity).

Air temperature and relative humidity were measured with appropriate sensors (model HMP-35A, Vaisala, Helsinki, Finland) and were place along side the flux instrumentation. Surface wetness was measured with a home-made, electrical conductivity plate (Weiss, 1990). Ancillary meteorological and soil physics data were acquired and logged on Campbell CR-21x data loggers (Logan, UT). These sensors were sampled once a second. One-half hour averages were calculated and stored on a computer, to coincide with the flux measurements.

2.3. Flux density computations

Vertical flux densities of CO_2 (F_c), latent (λE) and sensible heat (H) between the forest and the atmosphere are proportional to the mean covariance between vertical velocity (w') and the respective scalar (c') fluctuations (e.g. CO_2, water vapor, and temperature). Positive flux densities represent mass and energy transfer into the atmosphere and away from the surface and negative values denote the reverse. Numerical coordinate rotations of the three orthogonal wind axes were applied to align the vertical velocity measurement normal to the mean wind streamlines. CO_2 and water vapor flux covariances were corrected for density fluctuations arising from variations in temperature and humidity. Mass and energy flux covariances reported in this paper were computed for half-hour intervals. To do so, turbulent fluctuations were computed as the difference between stantaneous (x_i) and mean ($\bar{x}_i$) quantities. Mean values were determined in real-time, using a digital recursive filter (Kaimal and Finnigan, 1994):

$$\bar{x}_i = \alpha \bar{x}_{i-1} + (1 - \alpha) x_i \tag{2}$$

where $\alpha = \exp(-\Delta t/\tau)$, Δt is the sampling time increment and τ is the filter time constant. In this study, a 400 s time constant was used.

2.4. Model computations

If we expect to model mass and energy at the floor of a forest canopy with accuracy, soil energy exchange algorithms must be coupled to a canopy-scale micrometeorology model. This is because the inputs of energy and the meteorological conditions (air temperature, humidity, wind speed) at the soil surface depend upon how the forest canopy and atmosphere interact with one another.

The CANPOND model was used to compute fluxes of mass and energy at the floor of the forest canopy. CANPOND is a one-dimensional, multi-layer

biosphere-atmosphere gas exchange model that computes water vapor and CO_2 flux densities. The model is derived from the CANOAK and CANVEG models, which are described in Baldocchi and Meyers (1998). The micrometeorological module computes leaf and soil energy exchange, turbulent transfer, carbon and water vapor profiles and radiative transfer through the canopy. Environmental variables, in turn, drive the physiological modules that compute leaf photosynthesis, stomatal conductance, transpiration, and respiration by foliage and woody tissue, and soil CO_2 flux (respiration by roots and microbes).

The radiative transfer model calculates probabilities of sunlit and shaded area for leaves and the soil. It also calculates the flux densities of energy on those leaf and soil fractions in the photosynthetically active and near infrared wavebands. Clumping of shoots is considered by using the Markov probability function to compute the probability of beam penetration (Nilson, 1971; Chen, 1996). Information on radiative flux densities are used to calculate photosynthesis, leaf and soil energy balance, and turbulent transfer of CO_2, water vapor and sensible heat. Stomatal conductance is calculated as a function of assimilation, relative humidity and CO_2 concentration at the leaf surface. Turbulent diffusion and dispersion matrices were computed using Lagrangian theory. The model assumes a horizontally homogeneous canopy and temporally steady environmental conditions. This allows the conservation equation for CO_2 or water vapor to be expressed as the equality between the change in concentration with height and the diffusive source/sink strength. The diffusive source strength is modeled from leaf area density with respect to height, concentration difference between the air outside the laminar boundary layer of leaves and within stomata, boundary layer resistance to molecular diffusion, stomatal resistance and air density.

Flux densities of heat transfer and water evaporation at the soil/litter boundary and soil temperature profiles were computed with a 10-layer numerical soil heat transfer model (Campbell, 1985). Soil reflectivity in the photosynthetically active and near infrared wavebands were set at 0.10 and 0.25, respectively, on the basis of data from quartz sand (Bowker et al., 1985).

A resistance approach was used to compute soil evaporation and sensible heat flux densities (Mahfouf and Noilhan, 1991). The algorithm chosen to compute soil evaporation (E_s) was:

$$E_s = \frac{\rho(\varphi\, q_{sat}(T) - q_a)}{R_{soil} + R_a} \quad (g\,m^{-2}\,s^{-1}) \tag{3}$$

where R_{soil} is the resistance of soil to evaporation, R_a is the soil surface aerodynamic resistance, ρ is air density, φ is relative humidity of the soil matrix, q_a is the mixing ratio of air and q_{sat} is the saturated mixing ratio. The algorithm of Camillo and Gurney (1986) was used to compute soil resistance.

$$R_{soil} = 4104(w_s - w_g) - 805 \quad (s\,m^{-1}) \tag{4}$$

The variable w_s is the saturated volumetric water content. For sand, it equals $0.395\,m^3\,m^{-3}$. The other variable, w_g, represents the near surface volumetric water contents of the soil. For these computations, we assumed that the litter was perfectly dry, as no rain had occurred and, thereby, adopted a value of zero for w_g. Implementing these parameter values in Eq. (4) yielded a value of R_{soil} equal to $816\,s\,m^{-1}$.

The relative humidity of the soil pores was evaluated from thermodynamic principles (Mahfouf and Noilhan, 1991) as:

$$\varphi = \exp\left(\frac{g\Psi}{R_w T}\right) \tag{5}$$

g is the acceleration due to gravity, Ψ is the capillary potential, R_w is the gas constant for water vapor and T is absolute temperature. The capillary potential was computed using an algorithm from Clapp and Hornberger (1978).

$$\Psi = \Psi_{sat}\frac{w^{-b}}{w_{sat}} \quad (m) \tag{6}$$

where w is the volumetric soil water content and w_{sat} and Ψ_{sat} represent parameter values for the respective variables when the soil is saturated with water. For sand and field conditions (Table 2), we assumed w equaled $0.1\,m^3\,m^{-3}$, b was 4.05, and Ψ was -0.121 m. Combining Eqs. (8) and (9), we estimated that the soil relative humidity was about 0.1.

We found it necessary to account for thermal stratification when computing the soil surface aerodynamic resistance (R_a). We used the method reported by Daamen and Simmonds (1996).

$$R_a = \frac{(\ln(z/z_0))^2}{k^2 u}(1+\delta)^{\varepsilon} \quad (s\,m^{-1}) \tag{7}$$

where z is height of the lowest model layer, z_0 is the roughness length for the soil surface, k is von Karman's constant (0.40) and u is wind speed. The dimensionless term, δ, is:

$$\delta = \frac{5gz(T_s - T_a)}{T_a u^2} \quad (8)$$

T_s and T_a are soil and air temperatures, g is the acceleration due to gravity, ε is an empirical coefficient. It is equal to -0.75 when δ is greater than zero and is -2 when δ is less than zero.

3. Results and discussion

The eddy covariance method was originally developed for measuring mass, energy and momentum exchange in the atmospheric surface layer. Turbulence spectra within vegetation differ from those associated with fluid flow above the canopy due to short-circuiting of the inertial cascade (Baldocchi and Meyers, 1991) and the intermittency of turbulence that results from the strong wind shear at the top of the canopy (Kaimal and Finnigan, 1994). Consequently, there remains uncertainty as how applicable the eddy covariance method is under a forest. Questions that persist include issues relating to the shape of the power spectra and co-spectra, the stationarity of the canopy environment, energy balance closure, instrument placement, sensor separation, averaging time, and filtering time constants on the interpretation of turbulence measurements. In the following section we examine these issues as they relate to eddy covariance measurements under the jack pine and ponderosa pine forests.

3.1. Measurement and computation of flux covariances

3.1.1. Power spectra and co-spectra

Fourier transforms were applied to 30 min records of 10 Hz turbulence data to examine the spectral features of vertical velocity (w), air temperature (T) and humidity (q). Figs. 2 and 3 present data from representative cases that were measured under the ponderosa and jack pine stands, respectively. Panel A presents normalized power spectra for vertical velocity (w), air temperature (T) and humidity (q). Panel B presents

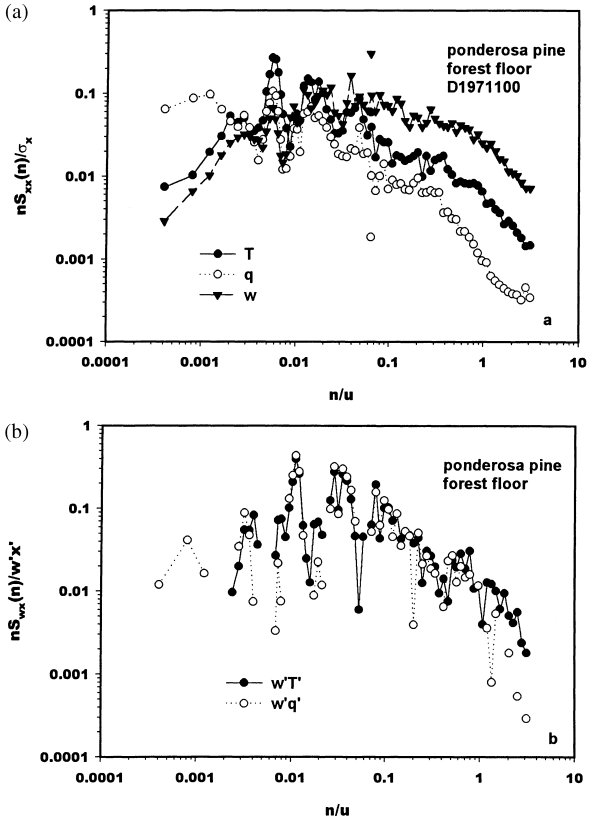

Fig. 2. (a) Power spectra for temperature (T), humidity (q) and vertical wind velocity (w) at 2 m above the ground in the understory of a ponderosa pine stand. The data were obtained at 11:00 hours on Day 197, 1996. The spectral density on the y axis is multiplied by natural frequency (n) and is normalized by the variance. The natural frequency on the x axis is divided by wind speed. On the assumption of Taylor's hypothesis, this metric approximates wavenumber ($1/\lambda$, m^{-1}). (b) Co-spectra for the covariances between vertical velocity and temperature ($\overline{w'T'}$) and humidity ($\overline{w'q'}$) at 2 m above the ground in the understory of a ponderosa pine stand. The spectral density on the y axis is multiplied by natural frequency (n) and is normalized by the covariance.

normalized co-spectra for the w–T and w–q covariances. To generalize, the power spectra and co-spectra spanned the wavenumbers (k) between 0.0004 and 10 m^{-1}. The power spectra and co-spectra possessed broad peaks in the wavenumber range between 0.01 and 0.1 m^{-1}. A spectral drop-off was observed at higher wavenumbers, a region that is typically associated with the inertial subrange. Most power spectra exhibited a short-circuiting of the inertial cascade (these slopes were steeper than the classical value of

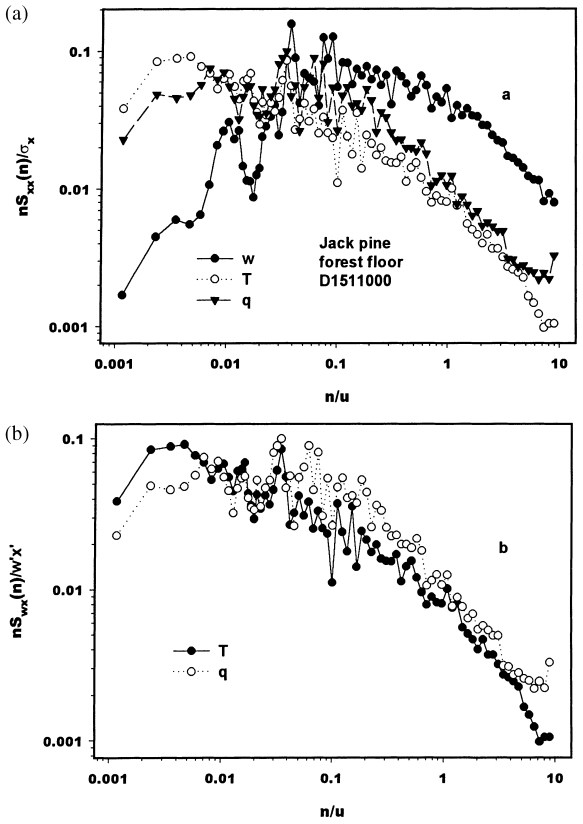

Fig. 3. (a) Power spectra for temperature (T), humidity (q) and vertical wind velocity (w) at 2 m above the ground in the understory of a jack pine pine stand. The data were obtained at 10:00 hours on Day 151, 1994. The spectral density on the y axis is multiplied by natural frequency (n) and is normalized by the variance. The natural frequency on the x axis is divided by wind speed. On the assumption of Taylor's hypothesis, this metric approximates wavenumber (k=1/λ, m^{-1}). (b) Co-spectra for the covariances between vertical velocity and temperature ($\overline{w'T'}$) and humidity ($\overline{w'q'}$) at 2 m above the ground in the understory of a jack pine stand. The spectral density on the y axis is multiplied by natural frequency (n) and is normalized by the covariance.

−2/3 for frequency adjusted spectra, $nS(n)$). In the ponderosa pine stand, the slopes of the w, u, T and q power spectra were −0.86, −0.95, −1.07 and −1.35, respectively. With respect to data from the jack pine stand, the slopes of the power spectra in the post-peak region were closer to values associated with surface boundary layer turbulence (e.g. Kaimal et al., 1972). The slopes for w, u, T and q were −0.67, −0.77, −0.90 and −0.79, respectively. In both studies, the vertical velocity-scalar co-spectra for temperature and humidity overlay one another. This result is expected when sources emanate from the same location, which in these cases the soil surface. Based on the information in these two figures, we conclude that we were able to measure most of the turbulent eddies that contribute to turbulence variances and covariances.

3.1.2. Transfer functions

Another way to examine errors is to examine spectral transfer functions for the effects of path averaging, sensor separation and sensor response and sampling times. Using the theory of Moore (1986), we present spectrally integrated correction factors for scalar covariances, $\overline{w'T'}$, $\overline{w'q'}$, and variances, $\overline{T'T'}$, and $\overline{q'q'}$ (Table 3). The spectrally-integrated correction factors are quite small, except for $\overline{w'q'}$, which is on the order of 1.2.

3.1.3. Mean removal and digital filters

Computations of flux covariances and variances are based on Reynolds' decomposition theory and involve removal of mean components. Traditionally one can perform this computation using arithmetic means, after the experiment, or with digital recursive filters on real-time data. As noted earlier, our experimental system uses digital filters. Theoretically, an optimal time constant can be chosen with the aid of a Fourier transform of the digital recursive filter:

$$|H(\omega)| = \frac{(1-\alpha)}{(1-2\alpha\cos(\omega T)+\alpha^2)^{0.5}} \quad (9)$$

where $H(\omega)$ is the filter transfer function, ω is the circular frequency (it equals 2π times the natural frequency, n) and T is the sampling interval. Comparing

Table 3
Spectral correction factors for a forest floor eddy covariance measurement system[a]

U ($m\,s^{-1}$)	$\overline{w'T'}$	$\overline{w'q'}$	$\overline{T'T'}$	$\overline{q'q'}$
0.10	1.009	1.223	1.014	1.049
0.15	1.012	1.227	1.006	1.048
0.25	1.009	1.223	1.007	1.047
0.50	1.010	1.224	1.012	1.048
1.00	1.010	1.224	1.018	1.049

[a] The algorithm of Moore (1986) are used. The sensor was at 2 m and the separation between the w and q sensor was 0.40 m. A spectrum for the surface boundary layer was used for these computations.

this equation with typical boundary layer co-spectra (Kaimal and Finnigan, 1994), we observe that over 90% of turbulent fluctuations contributing to the computation of the flux covariance are passed when digital time constants exceeding 200 s are employed.

We assessed the optimal time constant for sub-canopy turbulence measurements by comparing eddy covariances computed with the 400 s time constant against those computed with conventional Reynolds' decomposition, as averaged over 1 h. We observe little differences (within 1%) between the two methods of computing flux covariances (Fig. 4). Extending this analysis one step further, we compared flux covariances computed with the Reynolds' averaging technique against those computed using digital time constants that varied between 50 and 1500 s. Mass and energy flux covariance computations exhibited only a weak sensitivity to the choice of filter time constant (Table 4). An 800 s digital time constant was most ideal for computing flux covariances. Overall, time constants between 100 and 800 s yielded covariance values that agreed within 1% of the Reynolds' flux covariance, as averaged over 1 h.

3.2. Radiation field, flux footprints and energy balance closure

Sunlight received at the forest floor is the driving force for mass and energy exchange at this level. The distinct structure of ponderosa and jack pine forests made a sizable impact on the solar radiation field that was observed near the ground (Fig. 5). As expected, the light environment within both forests consisted of a mix of shade and sun patches. The size of the sun patches, however, differed considerably. Within the ponderosa pine stand, sun patches exceeded 5 m in length and the energy within them exceeded that in shade patches by more than 1000 μmol m^{-2} s^{-1}. In contrast, the dimension of typical sunflecks in the jack pine stand was generally less than 1 m. On

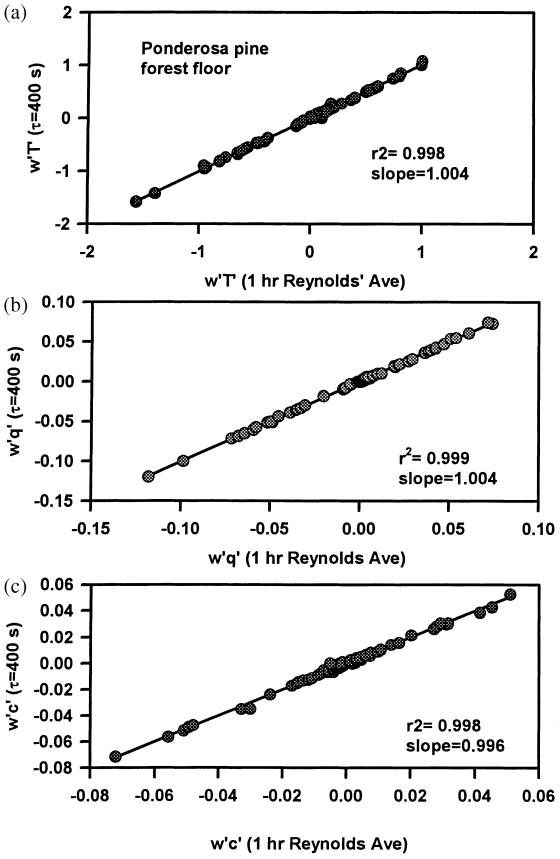

Fig. 4. A comparison between velocity-scalar eddy covariance calculated with different averaging methods. The *x*-axis is based on the Reynolds averaging technique and each datum represents the averaging of 10 Hz sampling over the duration of 1 h. The *y*-axis was computed using a digital recursive filter. A 400 s time constant was used for these calculations. (These data represent covariances between the raw voltages measured in the field. No calibration coefficients have been applied). The panels contain information on the vertical velocity-scalar covariances for (a) temperature; (b) humidity; (c) carbon dioxide.

Table 4
Slopes of the linear regression between covariances computed with the digital recursive filter method and those computed with conventional Reynolds' averaging[a]

τ	slope ($w'c'$)
50	0.989
100	0.9908
200	0.9949
300	0.9900
400	0.9970
600	0.9977
800	1.001
1000	1.002
1500	1.006

[a] The length of each time series was 3600 s. Ninety-nine runs were used in the analysis for different digital recursive time constants (τ).

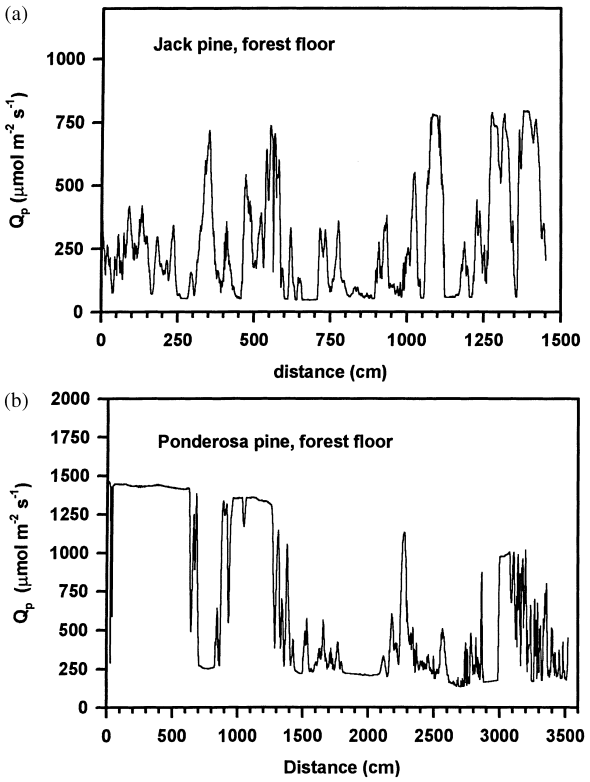

Fig. 5. The spatial variation of photosynthetically active radiation (Q_p) above the floor of (a) a boreal jack pine stand; (b) a temperate Ponderosa pine stand. The data measured in the jack pine stand came from Day 206, 1994, between 09:32 and 09:52 hours, CST. The mean value of Q_p across a 15 m domain was 269 mmol m^{-2} s^{-1}. The standard deviation was 217 mmol m^{-2} s^{-1}, the minimum and maximum flux densities were 47 and 796 mmol m^{-2} s^{-1}, respectively. The data measured in the ponderosa pine stand come from Day 194, 1996, between 1347 and 14:39 hours, PST. The mean value of Q_p across a 35 m domain was 674 mmol m^{-2} s^{-1}. The standard deviation was 499 mmol m^{-2} s^{-1}, the minimum and maximum flux densities were 135 and 1465 mmol m^{-2} s^{-1}, respectively.

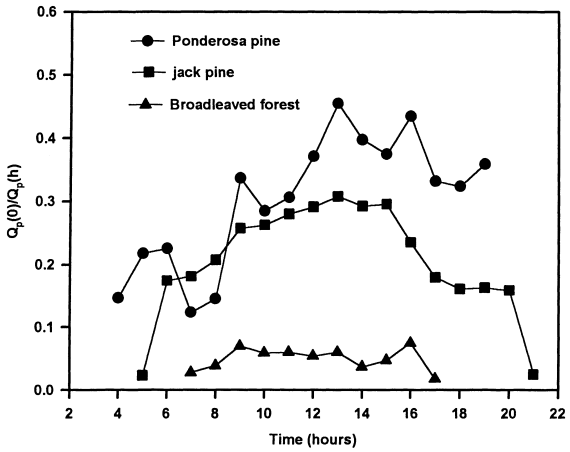

Fig. 6. The mean diurnal pattern of the transmission of photosynthetically active radiation (Q_p) to the floor of a temperate ponderosa pine, a boreal jack pine and a temperate broadleaved forest.

average, 40–50% of sunlight that is incident to the top of the canopy reaches the floor of the ponderosa pine stand, while about 30% of incident radiation reached the floor of the jack pine stand (Fig. 6). For comparison, less than 10% of incoming solar radiation reaches the floor of a temperate broad-leaved, deciduous forest (Baldocchi and Vogel, 1996).

With such heterogeneity of radiation near the forest floor, it is critical to quantify the scales of turbulence and the horizontal dimension of the flux footprint that is measured by an understory eddy covariance system. We can infer, from the power and co-spectra, that the dimension of large scale eddies, which range from 10 to 100 m. Hence to a first order, the largest eddies average across the largest sunflecks.

The dimensions of flux footprint source area near the forest floor were quantified with a two-dimensional Lagrangian diffusion footprint model (Baldocchi, 1997). The dimension of the forest floor source region (e.g. the 'flux footprint' is defined from the probability that fluid parcels, released at various distances upwind (x), cross the level (z) where a detector is placed. Theoretically, the 'flux footprint', under the ponderosa pine stand, ranges between 1 and 50 m upwind of the eddy covariance measurement system but the peak of the distribution is only 2 m upwind of the instrument mast (Fig. 7). Under the jack pine stand, the dimensions of the forest floor footprint are confined, theoretically, within 10 m of the eddy covariance measurement system.

Examination of surface energy balance is an exercise typically undertaken by micrometeorologists to test, independently, the accuracy and applicability of the eddy covariance method, when applied in ideal and non-ideal situations. How well the surface energy balance is closed under a forest canopy depends where the radiation tram and flux measurement systems are placed respective of one another, the length of the traversing tram system, and the dimensions of the flux

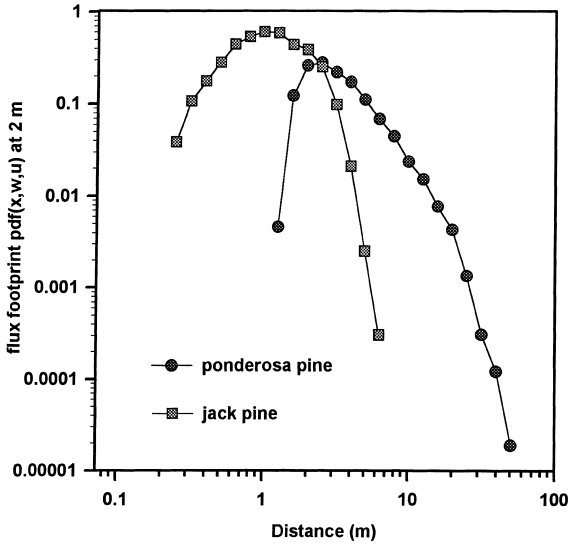

Fig. 7. Theoretical computations of the horizontal distribution of the 'flux footprint' probability density function, as measured at 2 m above the floor of a jack pine and a ponderosa pine. The footprint probability distributions were computed on the basis of Lagrangian theory, with a model that considered fluid parcel movement in the vertical and horizontal dimensions (Baldocchi, 1997). Wind parameters were set to match conditions that represent the mode of the probability distribution shown in Fig. 1.

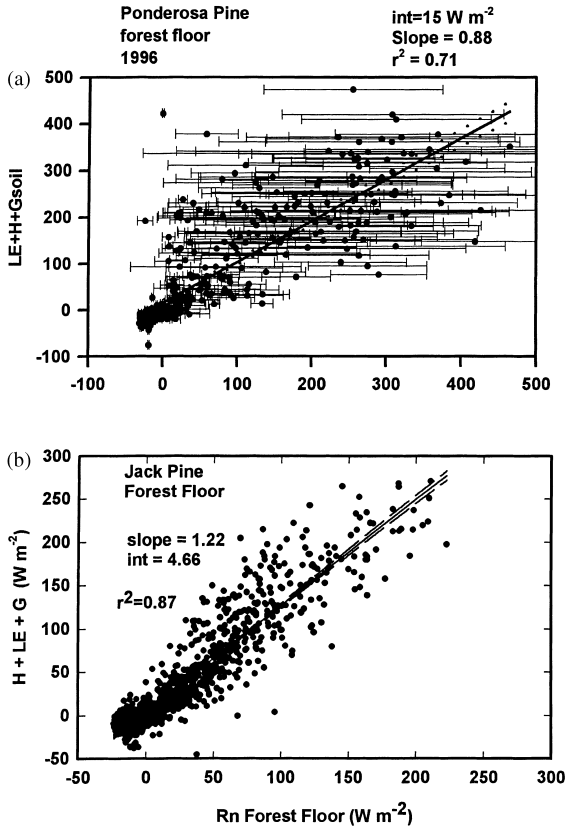

Fig. 8. Tests of energy balance closure at the floor of a ponderosa pine (a) and jack pine (b) forest. The net radiation flux density is compared against the summation of latent (λE), sensible (H) and conductive (G) heat flux densities.

footprint. Ideally, one would aim to obtain a spatially representative measure of the available energy within the flux footprint (see Schmid, 1997). In practice, this result is difficult to achieve as the dimensions of the footprint vary from run to run. Furthermore, it is very expensive to place the required number of radiometers within that spatial domain.

Fig. 8 shows how well the surface energy balance was closed under the ponderosa and jack pine forest stands. Under the ponderosa pine stand, the regression between the sum of the energy balance components — sensible heat (H), latent heat (λE) and soil heat (G) flux densities — and the net radiation balance (R_n) yielded a slope of 0.88 and an intercept of $15\,W\,m^{-2}$. When we moved the tram system to another area (not shown), the regression between $H+\lambda E+G$ and R_n changed, yielding a slope of 0.70 and an r^2 of 0.71. In contrast, the regression between $H+\lambda E+G$ and R_n, under the jack pine stand, resulted in a slope of 1.22 and an intercept of $4.66\,W\,m^{-2}$.

Large radiation gradients, over the space of tens of meters, can drive significant amounts of horizontal advection of energy within the sub-canopy air space of the ponderosa pine stand. Consequently, large bias and sampling errors were observed for hour by hour measurements, as quantified by the fact that only 71% of the variance in R_n is described by measurements of $H+\lambda E+G$ under the ponderosa pine stand. In contrast, the dimension of the flux footprint under the jack pine stand is large enough to average mass and energy exchange over several sun and shade patches. In this situation, about 87% of the variance in R_n was described by measurements of $H+\lambda E+G$. From these results, we conclude that the surface energy balance under a forest can be closed, on average, within plus/minus 25% of the measured net radiation balance. The precision of individual runs, on the other hand, is much lower. We also stress a need to have a horizontally

averaged measurement of the radiation field that corresponds with the dimensions of the flux footprint and the heterogeneity of the sub-canopy radiation field.

3.3. Turbulence and covariance statistics

The turbulent transfer of heat, momentum and matter is an intermittent process in the atmospheric surface layer (Sreenivasan et al., 1978). One would expect the intermittency to increase inside a plant canopy due to the presence of heterogeneous plant elements (Kaimal and Finnigan, 1994) and the noted mosaic of sunflecks and shade patches. A representative time trace of the vertical velocity–temperature covariance, also known as the kinematic heat flux density $\overline{w'T'}$, is shown in Fig. 9 to give the reader a qualitative impression of the temporal variability of turbulence measurements. These data were measured under the ponderosa pine stand during a nighttime and daytime period. During the day the transfer of heat, e.g. $\overline{w'T'}$, is associated with quiescent periods of varying duration (50–200 s) that are punctuated with short events when relatively large amounts of heat are transferred. At night, heat transfer is associated with rapid events, that transfer heat both upward and downward, and infrequent slow events that transfer heat downward. This behavior is consistent with observations reported by Paw U et al. (1992) and Lee et al. (1997). A quantitative analysis of temperature and heat transfer is presented in Fig. 10 by means of the mean diurnal pattern of three statistical moments, the coefficient of variation, skewness $\overline{x'^3}/\sigma^3$, and kurtosis, $\overline{x'^4}/\sigma^4$. On average the standard deviation of the *w–T* covariance, is between 10 and 100 times the mean. In contrast, fluctuations in temperature are typically less than 5% of the mean. With regard to higher order moments, the statistical behavior of temperature fluctuations was close to Gaussian, as skewness was near zero and kurtosis was near three. Heat

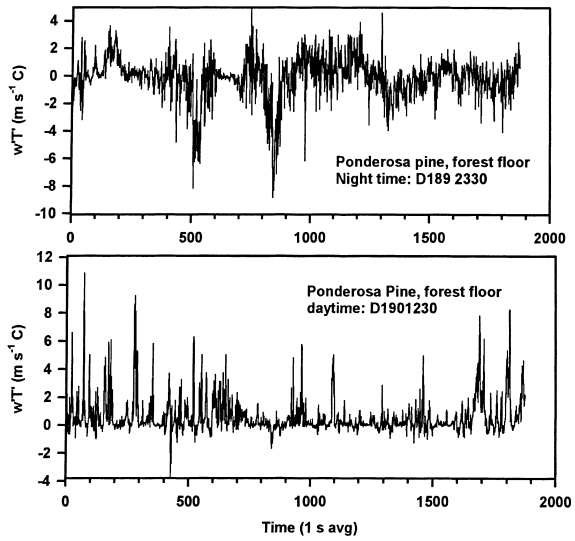

Fig. 9. A time trace of the vertical velocity–temperature covariance during a nighttime (Day 189, 23:30 hours) and a daytime (Day 190, 12:30 hours) period. The measurements were made at 2 m above the ground in the understory of a ponderosa pine stand.

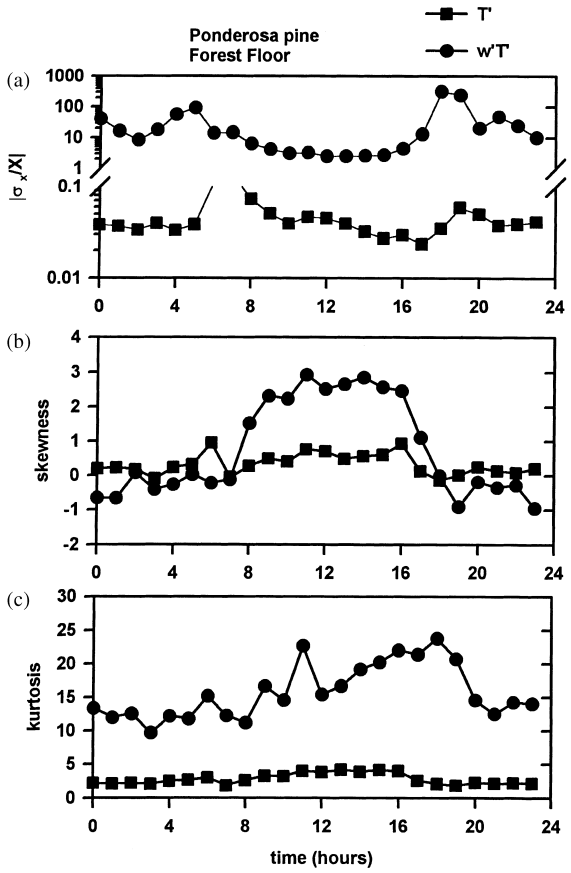

Fig. 10. Diurnal pattern of mean statistics associated with temperature fluctuations and the covariance between vertical velocity and temperature fluctuations in the understory of a ponderosa pine stand; (a) The coefficient of variation, the standard deviation divided by the mean; (b) Skewness, the third-order moment; (c) Kurtosis, the fourth-order moment.

transfer, on the other hand, was positively skewed and highly intermittent (Kr>10) during the day. At night, kurtosis remained high, but skewness approached zero. We note that a similar set of relation was observed for humidity and moisture transfer (not shown). These data suggest that temperature (and humidity) stationarity was attained in the sub-canopy even though the flux contributions are intermittent.

3.4. Diurnal variation of energy exchange near a forest floor

Mean diurnal patterns of R_n, H, λE and G for both stands are shown in Fig. 11. Data from a series of days were bin-averaged by hour. We used this method to reduce the sampling error associated with individual flux measurements that resulted from intermittent nature of turbulence and advection caused by horizontal transport across large sun and shade patches (Sreenivasan et al., 1978; Moncrieff et al., 1996). Mean

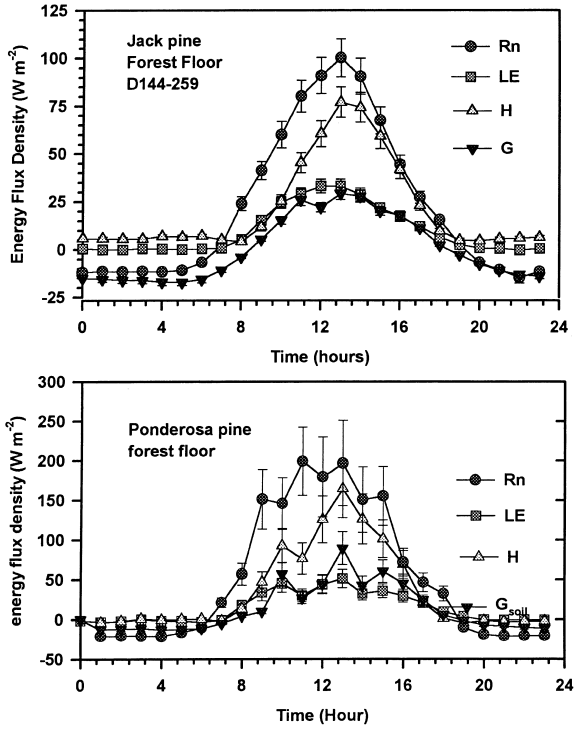

Fig. 11. The mean diurnal pattern of net radiation (R_n) and latent (λE), sensible (H) and conductive (G) heat flux densities at the soil surface of a jack pine and ponderosa pine forest.

energy fluxes at the floor of the ponderosa pine are nearly twice the magnitude of those observed under the jack pine. Mean mid-morning to mid-afternoon values of R_n, H, λE and G attain values are near 200, 150, 30 and 50 W m^{-2}, respectively, under the ponderosa pine stand. In comparison, mean mid-morning to mid-afternoon mean values of R_n, H, λE and G were about 100, 75, 25 and 20 W m^{-2}, respectively, under the jack pine stand. In general, twice as much available energy (R_n–G) was measured under the sparse ponderosa pine stand. The forest floor Bowen ($H/\lambda E$), however, was not conservative. A disproportionate amount of the extra available energy at the floor of the ponderosa pine stand was partitioned into driving sensible heat exchange. These large rates of sensible heat exchange maintain an unstable thermal stratification in the forest understory, during the day, as suggested by Leclerc et al. (1990).

3.5. Relationship between energy flux densities and environmental variables

Evaporation rates near the forest floor were conservative, as compared to values typically measured above the forest. Maximal values of λE over dry surfaces rarely exceeded 50 W m^{-2}, despite net radiation flux densities approaching 250 W m^{-2}. The conservative nature of forest floor latent heat exchange seems to be a common observation over dry soils under forests (Denmead, 1984; Baldocchi and Meyers, 1991; Moore et al., 1996; Blanken et al., 1997; Kelliher et al., 1998). In contrast, higher rates of evaporation, representing 66% of the local net radiation balance, can be observed over a transpiring vegetative understory (Blanken et al., 1997).

The relationship between available energy (R_n–G) and latent heat flux densities above the forest floor is shown in Fig. 12. Data were obtained from a spectrum of sparse and closed forest canopies to broaden the range. Soil latent heat flux densities increase linearly with available energy up to 100 W m^{-2}, where it reaches a threshold near about 35 W m^{-2}. In this range, soil evaporation is about one-quarter of available energy. As available energy exceeds this threshold, soil evaporation rates are unable to match the potential evaporative demand, as defined by available energy. This result is consistent with our earlier

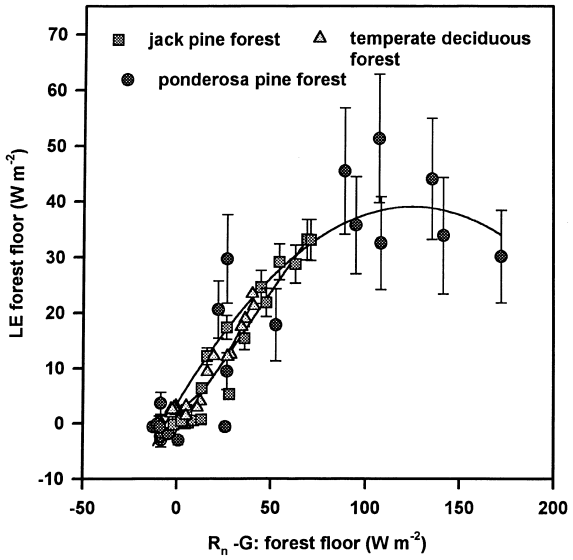

Fig. 12. The relationship between forest floor latent heat flux density and available energy.

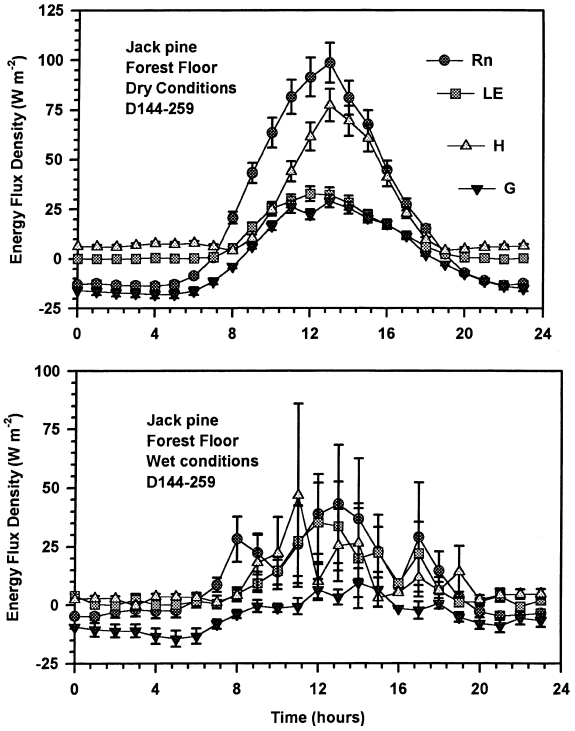

Fig. 13. The mean diurnal pattern of net radiation (R_n) and latent (λE), sensible (H) and conductive (G) heat flux densities at the soil surface of a jack pine forest. These data were obtained between Days 144 and 259, 1994. Panel A represents periods when the forest floor was dry. Panel B represents periods when the forest floor was wet.

finding (Baldocchi and Meyers, 1991). A feedback between the humidity deficit of the air, the surface evaporation rate and the available energy is responsible for this result. Large-scale and intermittent turbulent gusts displace the air in contact with the soil before the humidity deficit of a parcel of air comes into equilibrium with the potential soil evaporation rate, as determined by available energy.

The presence of surface wetness alters the interrelationship between R_n, λE, H and G. Fig. 13 shows that the ratio between λE and R_n, is closer to unity under the jack pine stand, when the forest floor is wet. The absolute value of λE at this site, however, is relatively unchanged whether the surface is wet or dry (midday λE remains near 25 W m^{-2}). What differs dramatically is the net radiation balance. The sky is cloudier during wet periods. This occurrence, thereby, limits R_n and the potential for high soil evaporation rates from an otherwise freely evaporating surface.

One draws a different conclusion when examining the mean diurnal pattern of energy exchange near the floor of the Ponderosa pine stand, during the spring of 1997, a period when frequent rainfall occurred (Fig. 14). Wetting of the soil surface under the Ponderosa pine resulted in a dramatic reversal of the Bowen ratio. The mean Bowen ratio changed from a mean value of 2.16, when to the surface was drying, to a value of 0.47, when the surface was wet. Dynamically, soil evaporation rates are expected to decrease with the square root of time after a rain event (Denmead, 1984; Kelliher et al., 1998). Our measurements were unable to test this idea, unfortunately.

3.6. Assessment of model computations of energy exchange near the forest floor

Fig. 15 shows a comparison between model computations and measurements of R_n, λE, H and G at the floor of the ponderosa pine stand. The diurnal pattern represents an ensemble of bin-averaged data that was obtained between Days 185 and 205, 1996. Again, hourly-based bin-averaging was used to conduct a representative model test. Despite the practical difficul-

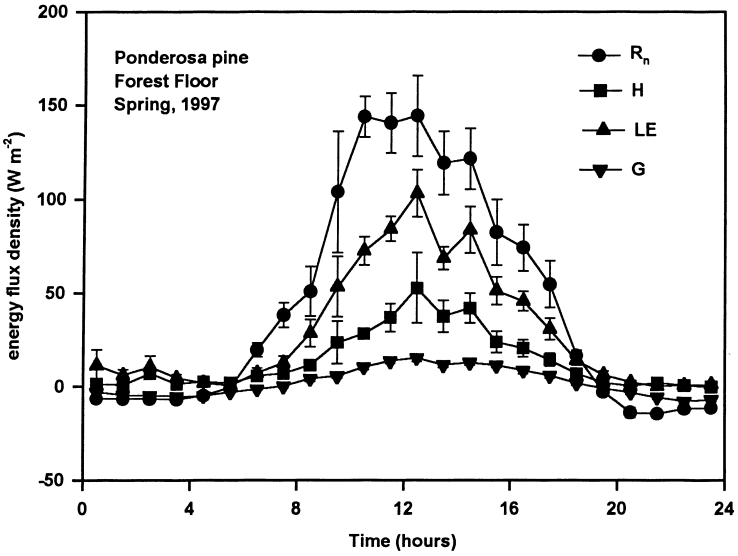

Fig. 14. The mean diurnal pattern of net radiation (R_n) and latent (λE), sensible (H) and conductive (G) heat flux densities at the soil surface of a ponderosa pine forest. These data were obtained during the spring of 1997 (Days 137–161) when rainfall was frequent (Days 143, 147, 14, 151, 154 and 155).

ties of making eddy flux measurements under a forest, the biophysical CANVEG model was able to simulate the mean diurnal patterns of R_n, λE, H and G well, for summertime conditions.

3.6.1. Using the CANVEG model to interpret field measurements

Any simulation of mass and energy exchange at the forest floor will be sensitive to model parameters that describe the aerodynamic and surface resistances and the physical properties of the soil. Our field data show that the magnitude of sensible heat flux density is very large at the soil surface of conifer forests and that the surface temperature can exceed air temperature by 10–15°C. Consequently, it is important to parameterize the surface aerodynamic resistance as a function of atmospheric thermal stability (Daamen and Simmonds, 1996). Fig. 16 shows how sensitive the diurnal pattern of soil surface energy flux densities is to different means of computing R_a. One case assumed neutral thermal stratification. The other case adjusted the soil aerodynamic resistance for the effects of thermal stratification, using the algorithm of Daamen and Simmonds (1996). Higher sensible heat flux densities were generated, using Eq. (8). This effect also resulted in lower net radiation, latent heat and soil heat flux densities. Non-realistic, negligible values of H occurred when R_a was not adjusted for thermal stratification, re-enforcing the need to incorporate this procedure into the model.

The depth of the litter layer also has an impact on energy partitioning, as it can insulate the highly conductive mineral soil layer from the atmosphere. A thicker litter layer produces lower G, but higher H and λE values (Fig. 17).

4. Summary and conclusions

The eddy covariance method can be a valid method for measuring mass and energy exchange above the soil surface of sparse and heterogeneous conifer forest stands, as long as certain precautions are taken. The heterogeneous nature these forest stands causes a large amount of spatial variability in sun and shade patches. Combined with intermittent turbulence, these factors will cause much spatial and temporal variability within the flux footprint that is being sampled. Consequently, flux covariances, determined from individual sampling periods, experience much run-to-run variability. On

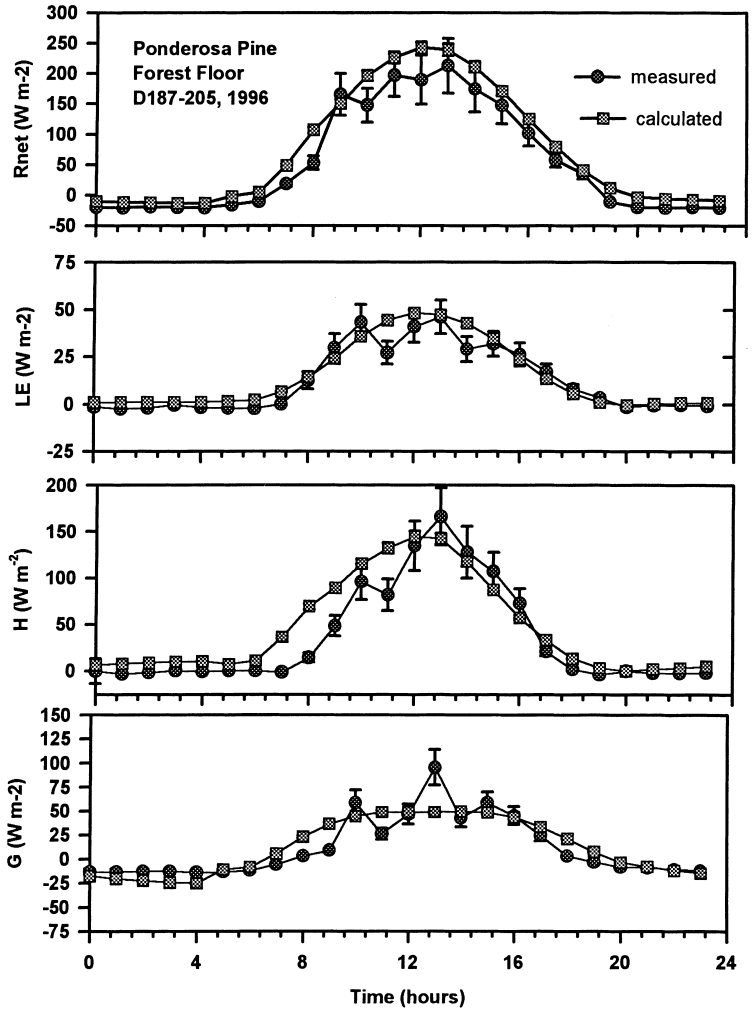

Fig. 15. A comparison between measured and calculated values of the mean diurnal pattern of net radiation (R_n) and latent (λE), sensible (H) and conductive (G) heat flux densities at the soil surface of a ponderosa pine forest. The calculations were derived from the CANPOND model.

the other hand, by bin-averaging many runs, by hour, we observe good agreement between turbulent energy fluxes and available energy (or model calculations). Thereby, the eddy covariance method seems to be a good means for studying the mean behavior of mass and energy exchange below forest canopies. Its non-obstructive nature enables it to study the physical processes that control mass and energy exchange under forests. For the cases studied here, evaporation rates from dry surfaces are related to available energy in a non-linear fashion. Evaporation rates over dry soil surfaces tend to reach a threshold of about $35\,W\,m^{-2}$ as the frequent occurrence of large turbulent wind gusts prevent the canopy air from reaching equilibrium with potential evaporation. The partitioning of solar energy into sensible, latent and soil heat flux is affected by atmospheric thermal stratification, surface wetness and the thickness of the litter layer.

We advocate the study of mass and energy exchange at multiple sites, which vary in canopy structure, as a means of studying the processes that control energy exchange of forest floors. For instance, the importance

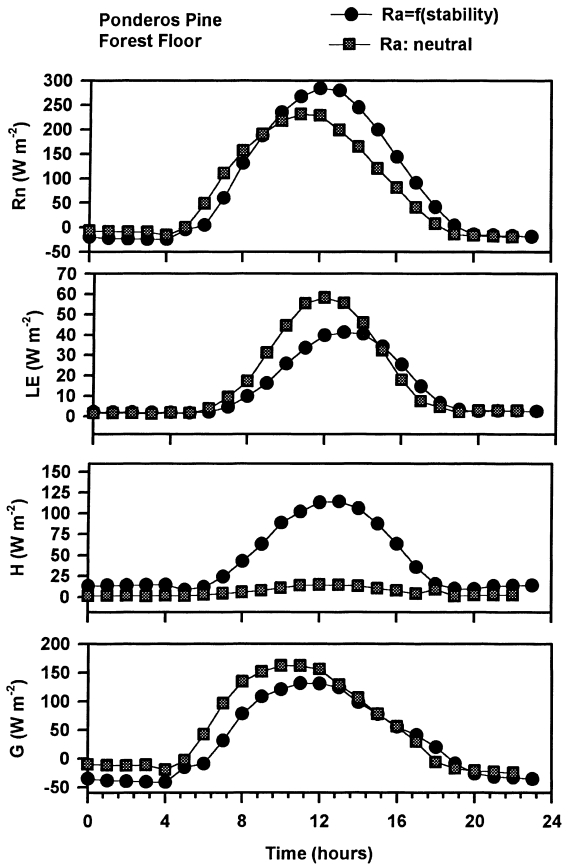

Fig. 16. The impact of the soil surface aerodynamic resistance on the mean diurnal pattern of net radiation (R_n) and latent (λE), sensible (H) and conductive (G) heat flux densities at the soil surface of a ponderosa pine forest. The calculations were derived from the CANPOND model. Cases are considered for situations when R_a is and is not a function of atmospheric stability.

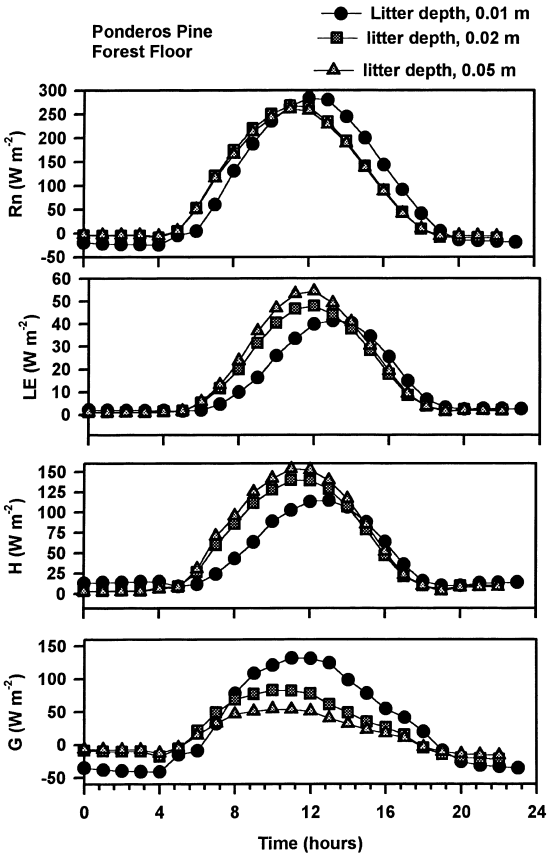

Fig. 17. The impact of varying litter depth on the mean diurnal pattern of net radiation (R_n) and latent (λE), sensible (H) and conductive (G) heat flux densities at the soil surface of a ponderosa pine forest. The calculations were derived from the CANPOND model.

of buoyancy on determining R_a was not drawn from our previous work in a dense temperate deciduous forest since H is near zero in that stand (Baldocchi and Vogel, 1996).

In conclusion, these data emphasize the importance of mass and energy exchange at the soil surface below sparse canopies. Big-Leaf models, for computing mass and energy fluxes, are bound to fail in these circumstances. Modelers should treat sparse forests as dual source systems, e.g. Norman et al. (1995). Our results also show that modelers need to consider such factors as litter depth and thermal stratification when modeling mass and energy exchange at the soil-air interface below forest crowns.

Acknowledgements

Portions of this work were funded by the NOAA Office of Global Programs (BOREAS) and NASA's Mission to Planet Earth.

We thank Mike Unsworth, Richard Vong, Mark Hall, Chris Vogel, David Auble and Robert Mayhew for experimental field assistance and/or instrument design and fabrication. Special thanks are expressed to Kell Wilson for his review of the manuscript and many valuable discussions on this topic and to Tilden

Meyers for the design of the solar panel energy system.

References

Auble, D.L., Meyers, T.P., 1992. An open path, fast response infrared absorption gas analyzer for H_2O and CO_2. Boundary Layer Meteorol. 59, 243–256.

Baldocchi, D.D., 1997. Flux footprints under forest canopies. Boundary Layer Meteorol. 85, 273–292.

Baldocchi, D.D., Meyers, T.P., 1991. Trace gas exchange at the floor of a deciduous forest I. Evaporation and CO_2 efflux. J. Geophys. Res. Atmos. 96, 7271–7285.

Baldocchi, D.D., Meyers, T.P., 1998. On using eco-physiological, micrometeorological and biogeochemical theory to evaluate carbon dioxide, water vapor and gaseous deposition fluxes over vegetation. Agric. For. Meteorol. 90, 1–26.

Baldocchi, D.D., Vogel, C., 1996. A comparative study of water vapor, energy and CO_2 flux densities above and below a temperate broadleaf and a boreal pine forest. Tree Physiol. 16, 5–16.

Baldocchi, D.D., Vogel, C.A., Hall, B., 1997. Seasonal variation of energy and water vapor exchange rates above and below a boreal jack pine forest canopy. J. Geophys. Res. 102, 28939–28951.

Black, T.A., Kelliher, F.M., 1989. Processes controlling understory evapotranspiration. Phil. Trans. R. Soc. Lond. B 324, 207–231.

Blanken, P.D., Black, T.A., Yang, P.C., Neumann, H.H., Nesic, Z., Staebler, R., den Hartog, G., Novak, M.D., Lee, X., 1997. Energy balance and canopy conductance of a boreal aspen forest: partitioning overstory and understory components. J. Geophys. Res. 102, 28915–28927.

Boulet, G., Raud, I., Vauclin, M., 1997. Study of the mechanisms of evaporation under arid conditions using a detailed model of the soil–atmosphere continuum. Application to the EFEDA I experiment. J. Hydrol. 193, 114–141.

Bowker, D.E., Davis, R.E., Myrick, D.L., Stacy, K., Jones, W.T., 1985. Spectral reflectance of natural targets for use in remote sensing studies. NASA Reference Publication 1139.

Braud, I., Noilhan, J., Bessemoulin, P., Mascart, P., Haverkamp, R., Vauclin, M., 1993. Bare-ground surface heat and water exchanges under dry conditions: observations and parameterization. Boundary Layer Meteorol. 66, 173–200.

Brenner, A.J., Incoll, L.D., 1997. The effect of clumping and stomatal response on evaporation from sparsely vegetated shrublands. Agric. For. Meteorol. 84, 187–206.

Camillo, P.J., Gurney, R.J., 1986. A resistance parameter for bare-soil evaporation models. Soil Sci. 141, 95–105.

Campbell, G., 1985. Soil Physics with BASIC, Transpor Models for Soil–Plant Systems. Elsevier, New York.

Cellier, P., Richard, G., Robin, P., 1996. Partition of sensible heat fluxes into bare soil and the atmosphere. Agric. For. Meteorol. 82, 245–265.

Chen, J.M., 1996. Optically-based methods for measuring seasonal variation of leaf area index in boreal conifer stands. Agric. For. Meteorol. 80, 135–164.

Choudhury, B., Monteith, J.L., 1988. A four-layer model for heat budget of homogenous land surfaces. Q. J. R. Meteorol. Soc. 114, 373–398.

Clapp, R., Hornberger, G., 1978. Empirical equations for some soil hydraulic-properties. Water Resources Res. 14 (4), 601–604.

Cuenca, R.H., Stangel, D.E., Kelly, S.F., 1997. Soil water balance in a boreal forest. J. Geophys. Res. Atmos. 102, 29355–29366.

Daamen, C.C., Simmonds, L.P., 1996. Measurement of evaporation from bare soil and its estimation using surface resistance. Water Resources Res. 32, 1393–1402.

Denmead, O.T., 1984. Plant physiological methods for studying evaporation: problems of telling the forest from the trees. Agric. Water Manage. 8, 167–189.

Elias, T.S., 1980. The Complete Trees of North America. Van Nostrand Reinhold Company, New York.

Franklin, J.F., Dyrness, C.T., 1973. Natural vegetation of Oregon and Washington. General Technical Report, PNW-8. Pacific Northwest Forest and Range Experiment Station, Portland, OR.

Kaimal, J.C., Wyngaard, J.C., Haugen, D.A. et al., 1972. Spectral characteristics of surface layer turbulence. Quart J. Royal Meteorol. Soc. 98, 563–589.

Kaimal, J.C., Finnigan, J.J., 1994. Atmospheric Boundary Layer Flows: Their Structure and Measurement. Oxford University Press, New York, 289 pp.

Kelliher, F.M., Hollinger, D.Y., Schulze, E.D. et al., 1997. Evaporation from an eastern Siberian larch forest. Agric. For. Meteorol. 85: 135–148.

Kelliher, F.M., Lloyd, J., Arneth, A., Byers, J.N., McSeveny, T.M., Milukova, I., Grigoriev, S., Panfyorov, M., Sogatchev, A., Varlargin, A., Ziegler, W., Bauer, G., Schulze, E.D., 1998. Evaporation from a central Siberian pine forest. J. Hydrol. 205, 279–296.

Kelliher, F.M., Whitehead, D., McAneney, K.J., Judd, M.J., 1990. Partitioning evapotranspiration into tree and understory components in tow young *Pinus radiata*, D. Don stands. Agric. For. Meteorol. 50, 211–227.

Kondo, J., Saigusa, N., Sato, T., 1990. A parameterization of evaporation from bare soil surfaces. J. Appl. Meterol. 29, 385–389.

Law, B.E., Baldocchi, D.D., Anthoni, P.M., 1999a. Below canopy and soil CO_2 fluxes in a ponderosa pine forest. Agric. For. Meteorol. 94, 171–188.

Law, B.E., Ryan, M.G., Anthoni, P.M., 1999b. Seasonal and annual respiration of a ponderosa pine ecosystem. Global Change Biol. 5, 169–182.

Law, B.E., Waring, R.H., Anthoni, P.M., Aber, J.D., 2000. Measurements of gross and net ecosystem productivity and water vapor exchange of a *Pinus ponderosa* ecosystem, and an evaluation of two generalized models, Global Change Biol., in press.

Leclerc, M., Beissner, K.C., Shaw, R.H., den Hartog, G., Neumann, H.H., 1990. The influence of atmospheric stability on the budgets of the Reynolds stress and turbulent kinetic energy within and above a deciduous forest. J. Appl. Meteorol. 29, 916–933.

Lee, X., Neuman, H., den Hartog, G., Fuentes, J. et al., 1997. Observations of gravity waves in a boreal forest. Boundary Layer Meteorol. 84, 383–398.

Mahfouf, J.F., Noilhan, J., 1991. Comparative study of various formulations of evaporation from bare soil using in situ data. J. Appl. Meteorol. 30, 1354–1365.

Milhailovic, D.T., Rajkovic, B., Dekic, L., Pielke, R.A., Lee, T.J., Ye, Z., 1995. The validation of various schemes for parameterizing evaporation from bare soil for use in meteorological models: a numerical study using in situ data. Boundary Layer Meteorol. 76, 259–289.

Milhailovic, D.T., Kallos, G., 1997. A sensitivity study of a coupled soil–vegetaion boundary layer scheme for use in atmospheric modelling. Boundary Layer Meteorol. 82, 283–315.

Moncrieff, J.B., Mahli, Y., Leuning, R., 1996. The propagation of errors in long term measurements of land atmosphere fluxes of carbon and water. Global Change Biol. 2, 231–240.

Moore, C.J., 1986. Frequency response corrections for eddy covariance systems. Boundary Layer Meteorol. 37, 17–35.

Moore, K.E., Fitzjarrald, D.R., Sakai, R.K., Goulden, M.L., Munger, J.W., Wofsy, S.C., 1996. Seasonal variation in radiative and turbulent exchange at a deciduous forest in central Massachusetts. J. Appl. Meteorol. 35, 122–134.

Nilson, T., 1971. A theoretical analysis of the frequency of gaps in plant stands. Agric. Meteorol. 8, 25–38.

Norman, J.M., Kustas, W.P., Humes, K., 1995. A two-source approach for estimating soil and vegetation energy fluxes from observations of directional radiometric surface temperatures. Agric. For. Meteorol. 77, 263–293.

Paw U, K.T., Brunet, Y., Collineau, S., et al., 1992. On coherent structures in turbulence above and within agricultural plant canopies. Agric. For. Meteorol. 61, 55–68.

Penman, H.L., 1948. Natural evaporation from open water, bare soil and grass. Proc. R. Soc. Lond. A 193, 120–145.

Philip, J.R., 1957. Evaporation and moisture and heat fiels in soil. J. Meteorol. 14, 354–366.

Ritchie, J.T., 1972. Model for predicting evaporation from a row crop with incomplete cover. Water Resources Res. 8, 1204–1213.

Ross, J., 1976. Radiative transfer in plant communities. In: Monteith, J.L. (Ed.), Vegetation and the Atmosphere, 2. Academic Press, London, pp. 13–55.

Runyon, J., Waring, R.H., Goward, S.N., Welles, J.M., 1994. Environmental limits on net primary production and light-use efficiency across the Oregon transect. Ecol. Applications 4, 226–237.

Sauer, T.J., Norman, J.M., Tanner, C.B., Wilson, T.B., 1995. Measurement of heat and vapor transfer coefficients at the soil surface beneath a maize canopy using source plates. Agric. For. Meteorol. 75, 161–190.

Saugier, B., Granier, A., Pontailler, J.Y., Dufrene, E., Baldocchi, D.D., 1997. Transpiration of a boreal pine forest, measured by branch bags, sapflow and micrometeorological methods. Tree Physiol. 17, 511–520.

Schmid, H.P., 1997. Experimental design for flux measurements: matching scales of observations and fluxes. Agric. For. Meteorol. 87, 179–200.

Sellers, P.J., Dickinson, R.E., Randall, D.A., et al., 1997. Modeling the exchanges of energy, water, and carbon between continents and the atmosphere. Science 275, 502–509.

Shuttleworth, W.J., 1991. Evaporation models in hydrology. In: Schmugge, T.J., Andre', J.C. (Eds.), Land Surface Evaporation: Measurements and Parameterization. Springer, Berlin, pp. 93–120.

Shuttleworth, W.J., Wallace, J.S., 1985. Evaporation from sparse crops — an energy combination theory. Q. J. R. Meteorol. Soc. 111, 839–855.

Smith, W.K., 1985. Western montane forests. In: Chabot, B.F., Mooney, H.A. (Eds.), Physiological Ecology of North American Plant Communities. Chapman & Hall, New York, pp. 95–121.

Sreenivasan, K.R., Chambers, A.J., Antonia, R.A., 1978. Accuracy of moments of velocity and scalar fluctuations in the atmospheric surface layer. Boundary Layer Meteorol. 14, 341–359.

Villalobos, F.J., Fereres, E., 1990. Evaporation measurements beneath corn, cotton and sunflower canopies. Agron. J. 82, 1153–1159.

Wallace, J.S., Lloyd, C.R., Sivakumar, M.V.K., 1993. Measurements of soil, plant and total evaporation from millet in Niger. Agric. For. Meteorol. 63, 149–169.

Walker, G.K., 1983. Measurement of evaporation from soil beneath crop canopies. Can. J. Soil Sci. 63, 137–141.

Weiss, A., 1990. Leaf wetness: measurements and models. Remote Sensing Rev. 5, 215–224.

Zhao, C.L., Tans, P.P., Thoning, K.W., 1997. A high precision manometric system for absolute calibrations of CO_2 in dry air. J. Geophys. Res. 102, 5885–5894.